Accepted Manuscript online: 2021-09-07 Article published online: 2021-10-15

Incorporating Cyano Groups to a Conjugated Polymer Based on Double B←N-Bridged Bipyridine Units for Unipolar n-Type Organic Field-Effect Transistors

Xu Cao[a,b,$]
Yang Min[a,c,$]
Hongkun Tian[a]
Jun Liu*[a,b]

[a] State Key Laboratory of Polymer Physics and Chemistry, Changchun Institute of Applied Chemistry, Chinese Academy of Sciences, Changchun, 130022, P. R. of China
[b] University of Science and Technology of China, Hefei, 230023, P. R. of China
[c] University of Chinese Academy of Sciences, Beijing, 100049, P. R. of China
liujun@ciac.ac.cn
[$] These authors contributed equally to this work.

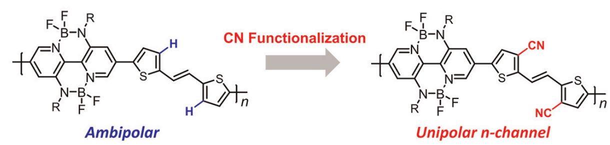

Received: 24.07.2021
Accepted after revision: 02.09.2021
DOI: 10.1055/a-1639-2383; Art ID: OM-2021-07-0037-OA

Abstract The development of n-type semiconductors lags far behind that of their p-type counterparts, demonstrating the exploration of exclusive *n*-type π-conjugated polymers is significant. The double B←N-bridged bipyridine (BNBP)-based polymers **P-BNBP-TVT** containing (*E*)-1,2-di(thiophen-2-yl)ethene (TVT) previously reported exhibits ambipolar character because of the electron-rich nature. Herein, we incorporated strong electron-withdrawing cyano groups into the 3,3′-positions of the TVT moiety to a copolymer **P-BNBP-2CNTVT** to develop n-type π-conjugated polymers. The LUMO/HOMO energy levels of **P-BNBP-2CNTVT** are −3.80/−5.95 eV, respectively, which are ~0.4 eV lower than that of **P-BNBP-TVT** without cyano groups. Unsurprisingly, compared with ambipolar **P-BNBP-TVT**, the organic field-effect transistors (OFETs) based on **P-BNBP-2CNTVT** showed unipolar n-type characteristics with an electron mobility of 0.026 $cm^2 \cdot V^{-1} \cdot s^{-1}$ and a lower threshold voltage of ~25 V as well as high I_{on}/I_{off} of ~10^5. This study demonstrates that organoboron π-conjugated polymers could be regarded as a tool for constructing exclusive n-type semiconducting polymers used in OFETs.

Key words: π-conjugated polymers, cyano-functionalization, organic field-effect transistors, electron transports, n-type polymer semiconductors

Introduction

π-Conjugated polymers have attracted increasing attention for their potential applications in organic electronic devices due to their advantages of low cost and flexibility.[1] Organic field-effect transistors (OFETs), one of the vital components of organic electronics, have been a hot topic because of their wide use in integrated circuits, displays, memory storage, skin sensors and so forth.[2] Over the past three decades, significant progresses have been made in the state-of-the-art p-type semiconducting polymers in OFETs with impressive hole mobilities of higher than 10 $cm^2 \cdot V^{-1} \cdot s^{-1}$.[3] However, the evolution of n-type semiconducting polymers still lags far behind that of their p-type counterparts, which is mainly attributed to the deficiency of π-conjugated polymers with high electron affinity and electron mobility. This unbalanced hole and electron mobilities will inevitably become an obstacle to organic complementary inverters and complementary logic circuits constructed with organic p–n junctions.[4] Therefore, it is imperative to explore the high-performance n-type semiconducting polymers by rational molecular designs.

The dominating challenges in achieving effective electron transport in polymer semiconductors consist in the implementation of sufficiently low-lying LUMO/HOMO energy levels. The deep LUMO energy levels could enhance the electron injection from the electrodes and facilitate the stable electron transport, and a low enough HOMO energy levels can also block the hole injection and accumulation. However, it is proverbial that a number of high-mobility polymers based on naphthalene diimide (NDI),[5] diketopyrrolopyrrole (DPP)[6] and isoindigo (IID)[7] exhibit ambipolar transport characteristics in OFETs, even though they typically contain electron-withdrawing imide- and amide-substituted

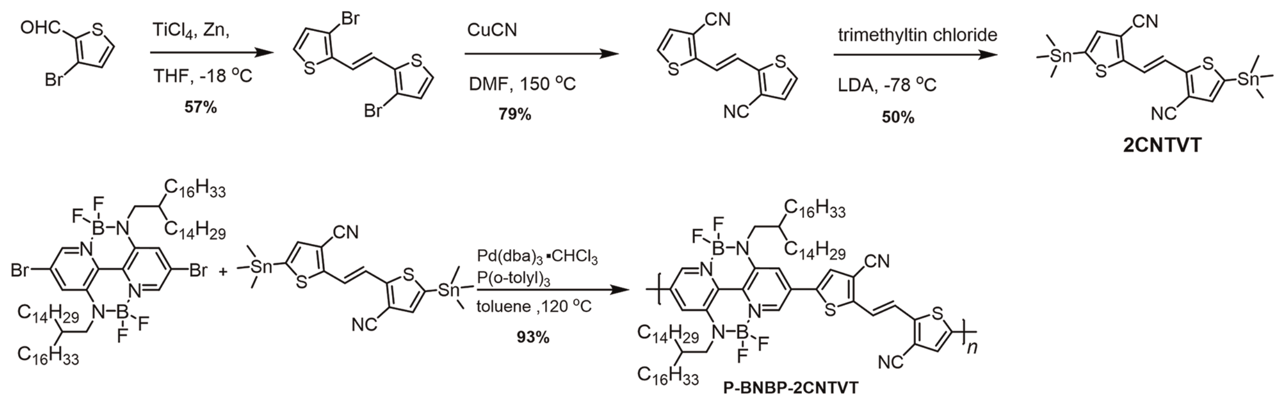

Scheme 1 Synthetic route of **P-BNBP-2CNTVT**.

groups. Conventionally, replacing hydrogen atoms in the backbone with strong electron-withdrawing groups including halogens (fluorine atoms and chlorine atoms)[8] and cyano moiety[9] could deepen the LUMO/HOMO energy levels further, which has been regarded as a facile and promising strategy to design exclusive n-type polymers. For example, Gao et al.[7a] reported that the multifluorination of IID-based polymers shows a conversion of ambipolar to n-type with a high electron mobility up to 4.97 $cm^2 \cdot V^{-1} \cdot s^{-1}$. Kim et al.[10] also reported an electron mobility of 1.20 $cm^2 \cdot V^{-1} \cdot s^{-1}$ for DPP-based polymers containing cyano groups.

A highly π-extended (*E*)-1,2-di(thiophen-2-yl)ethene (TVT) unit is a versatile building block for high-performance polymers because of its good coplanarity to promote intrachain charge transport.[11] On the other hand, there are a lot of copolymers based on the TVT unit having p-type or ambipolar character owing to its electron-rich nature.[3a,12] In our previous study,[13] we copolymerized the electron-deficient double B←N-bridged bipyridine (BNBP) with the TVT unit, and the corresponding copolymer (**P-BNBP-TVT**) exhibits ambipolar character due to the high-lying LUMO/HOMO energy levels. To lower the frontier energy levels, herein, we introduced cyano groups at the 3,3′-positions of the TVT moiety to successfully synthesize the copolymer, **P-BNBP-2CNTVT**. As we expected, the strong electron-withdrawing nitrile moieties could dramatically enhance the electron affinity of the copolymers. CV measurements verified that **P-BNBP-2CNTVT** shows lower LUMO/HOMO energy levels of −3.80 eV/−5.95 eV, respectively, which are much lower than those of **P-BNBP-TVT**. The difference with ambipolar **P-BNBP-TVT** is that the OFETs based on **P-BNBP-2CNTVT** exhibit exclusive n-type charge transport with a moderate electron mobility of 0.026 $cm^2 \cdot V^{-1} \cdot s^{-1}$.

Results and Discussion

Synthesis and Characterizations. The chemical structures of **P-BNBP-TVT** and **P-BNBP-2CNTVT** are shown in Figure 1. We decorated the cyano groups at the 3,3′-positions of the TVT unit to construct a promising n-type π-conjugated polymer based on the BNBP unit. **P-BNBP-TVT** has been reported in our previous study.[13] The synthetic route of **P-BNBP-2CNTVT** is depicted in Scheme 1, and the detailed synthetic procedures are provided in the Supporting Information. In terms of the syntheses reported, the monomer of **2CNTVT** was successfully prepared under the treatment of lithium diisopropylamine (LDA), then we performed the Stille-coupling polymerization between the monomer of **BNBP** and the monomer of **2CNTVT**. The long and branched alkyl chain 2-tetradecyloctadecyl was used to ensure the solubility. The crude product was purified by sequential Soxhlet extraction with acetone, n-hexane and chloroform to obtain the desired copolymer **P-BNBP-2CNTVT** with 93% yield. Expectedly, **P-BNBP-2CNTVT** exhibits good solubility in common solvents, such as chloroform, chlorobenzene (CB), *o*-dichlorobenzene and so on, so that we carried out ^1H NMR to confirm the chemical structure. And the number-average molecular weight (M_n) and polydispersity index (PDI) of the copolymer are estimated by gel permeation chromatography (GPC) using distribution polystyrene as a standard. The molecular weight (M_n) of **P-BNBP-2CNTVT** is 51.5 kDa with a

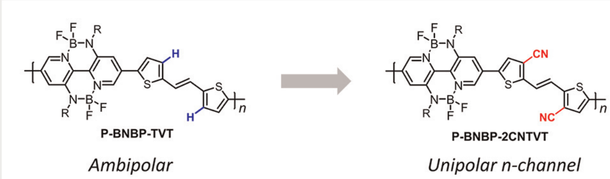

Figure 1 Molecular design and chemical structures of the polymers P-BNBP-TVT and P-BNBP-2CNTVT.

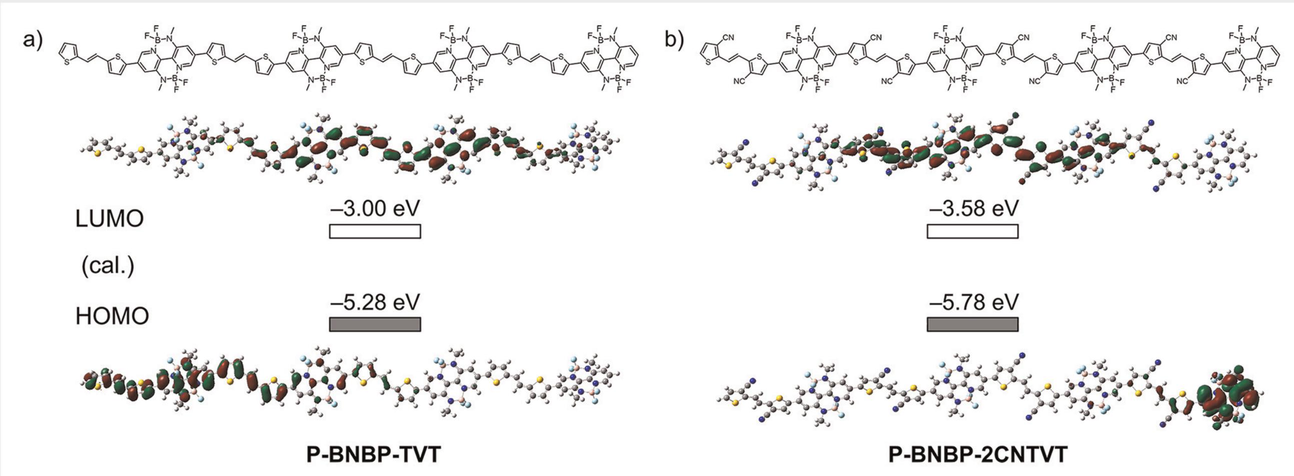

Figure 2 Molecular structures, Kohn–Sham LUMO and HOMO and their energy levels for the tetramer model compounds of a) **P-BNBP-TVT** and b) **P-BNBP-2CNTVT** calculated at the B3LYP/6–31 G(d,p) level of theory.

Table 1 Molecular, photophysical and electrochemical properties of **P-BNBP-TVT** and **P-BNBP-2CNTVT**

Polymer	M_n[a] [kg · mol^{-1}]	PDI	$\lambda_{max, sol}$[b] [nm]	$\lambda_{max, film}$[c] [nm]	E_g^{opt}[d] [eV]	E_{onset}^{red} [V]	E_{onset}^{ox} [V]	E_{LUMO}[e] [eV]	E_{HOMO}[e] [eV]
P-BNBP-TVT[13]	41.6	4.35	653	652	1.84	−1.40	+0.85	−3.40	−5.65
P-BNBP-2CNTVT	51.5	1.91	628	627	1.88	−1.0	+1.15	−3.80	−5.95

[a]M_n and PDI of the polymers were determined by GPC using polystyrene standards in TCB at 150 °C. [b]Measured in diluted CB solutions (10^{-5} M) at 25 °C. [c]Measured in thin films. [d]Calculated from the absorption band edge of the polymer films, $E_g = 1240/\lambda_{edge}$. [e]LUMO and HOMO energy levels were determined from the first reduction potential (E_{onset}^{red}) and oxidation potential (E_{onset}^{ox}) (vs. Fc/Fc$^+$) with the equations of $E_{LUMO}/E_{HOMO} = -(4.80 + E_{onset}^{red}/E_{onset}^{ox})$ eV.

PDI of 1.91 (Figure S2), which is comparable that of with **P-BNBP-TVT.**[13] **P-BNBP-2CNTVT** displays good thermal stability with a thermal decomposition temperatures (T_d, 5% weight loss) of 334 °C, as measured by thermogravimetric analysis under a nitrogen atmosphere (Figure S3). The differential scanning calorimetry scans of **P-BNBP-2CNTVT** show no melting or glass transitions in the 25–250 °C range (Figure S4).

Molecular Geometry and Electronic Structures. In order to elucidate the influences on polymer backbone configurations and electronic structures after incorporating cyano groups, density functional theory (DFT) calculations of two model tetramers (**P-BNBP-TVT** and **P-BNBP-2CNTVT** containing four repeating units) were performed at the B3LYP/6–31 G level of theory. The long alkyl side chains were replaced with methyl groups to simplify the calculations, and the results are shown in Figures 2 and S1. For **P-BNBP-TVT**, the torsion angle between BNBP and TVT is 22°; however, after the introduction of cyano groups, the torsion angle between BNBP and 2CNTVT is up to 27°, demonstrating negative influences on the molecular configuration due to the large steric hindrance of the cyano groups (vide infra). Although with the twisty backbone, the LUMO of **P-BNBP-2CNTVT** remains delocalized along the conjugated backbone, which is the same as that of **P-BNBP-TVT.** However, the HOMO of **P-BNBP-2CNTVT** is mainly localized on the BNBP moiety as compared with **P-BNBP-TVT**, in which the HOMO is delocalized along the conjugated backbone, indicating the strong electron-withdrawing properties of cyano groups. Further, **P-BNBP-2CNTVT** based on DFT calculations exhibits deeper LUMO/HOMO energy levels of −3.58 eV/−5.78 eV than those of **P-BNBP-TVT** of −3.00 eV/−5.28 eV. The results demonstrate that cyano-functionalization on the TVT moiety dramatically lowers the LUMO/HOMO energy levels, which could effectively enhance electron injection and block the hole injection to ensure the exclusively n-type transport character.

Photophysical and Electrochemical Properties. The UV-vis absorption spectra of **P-BNBP-TVT** and **P-BNBP-2CNTVT** in diluted CB solutions with the concentration of 10^{-5} M and in thin films are shown in Figure 3. The corresponding photophysical characteristics are summarized in Table 1. Both the absorption spectra of **P-BNBP-TVT** and **P-BNBP-2CNTVT** in CB solutions at room temperature exhibit the similar shape to their absorption spectra of thin films. In addition, the maximum absorption peaks of the two copolymers are almost impervious from the solutions to thin films, which demonstrates the strong pre-aggrega-

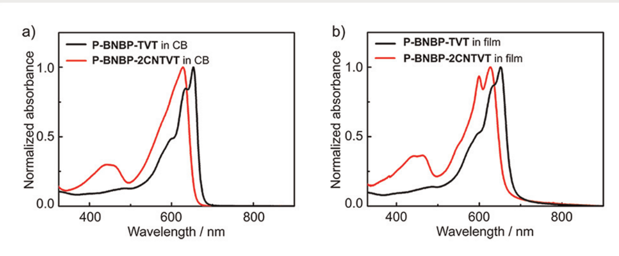

Figure 3 Normalized UV-vis absorption spectra of **PBNBP-TVT** and **P-BNBP-CNTVT** in their a) diluted CB solutions (10^{-5} M) and b) thin films.

tion in the solutions. The pre-aggregation characteristics further could be confirmed by the temperature-dependent absorption spectra shown in Figure S5. The maximum absorption peaks gradually blue-shift with the increasing temperature of the solution, along with the reduction of the absorption peak intensity. It is worth mentioning that the absorption spectra of **P-BNBP-2CNTVT** attaching cyano groups display a hypochromic shift in comparison to that of **P-BNBP-TVT**, and the maximum absorption peaks (λ_{max}) of **P-BNBP-TVT** and **P-BNBP-2CNTVT** are 653 nm and 623 nm, respectively. This could be mainly attributed to the weak intramolecular charge transfer character after the cyano-functionalization leading to a significant decrease of electron-donating ability of the TVT moiety.[6d,14]

To investigate the electrochemical properties of **P-BNBP-TVT** and **P-BNBP-2CNTVT**, we carried out film CV measurements using ferrocene/ferrocenium (FC/FC$^+$) as the internal standard, and a solution of 0.1 M tetrabutylammonium hexafluorophosphate ($TBAPF_6$) in acetonitrile was employed as the electrolyte. The CV curves are displayed in Figure 4. Both of the two copolymers exhibit obvious reduction and oxidation processes. On the basis of the onset potentials, the LUMO/HOMO energy levels are estimated to be −3.40 eV/−5.65 eV for **P-BNBP-TVT** and −3.80 eV/−5.95 eV for **P-BNBP-2CNTVT**, respectively. Obviously, the LUMO/HOMO energy levels of **P-BNBP-2CNTVT** dramatically decrease by 0.4 eV and 0.3 eV compared with those of **P-BNBP-TVT**, respectively, which demonstrates that the introduction of two strong electron-withdrawing cyano groups in the TVT moiety effectively lowers the LUMO/HOMO energy levels. The experimental LUMO/HOMO energy levels of the two copolymers are in good agreement with the theoretical calculations. The deeper LUMO/HOMO energy levels of **P-BNBP-2CNTVT** are expected to enhance the electron injection from the electrodes and generate a hole injection barrier.[15] These results strongly imply that **P-BNBP-2CNTVT** is going to be a promising candidate for exclusively electron transport materials.

OFET Performance. P-BNBP-2CNTVT possesses low-lying LUMO/HOMO energy levels, which strongly motivates us to investigate the charge-transporting properties of the copolymer. The solution-processed OFETs with the top-gate/bottom-contact (TGBC) configuration were fabricated. Figure 5 illustrates the representative transfer and output characteristics of the OFETs. The detailed device optimization processes by different annealing temperatures are shown in Figure S6 and Table S1. Expectedly, in comparison to **P-BNBP-TVT** showing ambipolar character, **P-BNBP-2CNTVT** exhibits typical unipolar n-type transport characteristic because of the deep LUMO/HOMO energy levels enhancing the electron injection and restricting hole injection after introducing cyano groups. And the maximum electron mobility (μ_e) of **P-BNBP-2CNTVT** extracted in the saturation regime is up to 0.026 $cm^2 \cdot V^{-1} \cdot s^{-1}$ with high I_{on}/I_{off} of 10^5 after thermal annealing at 200 °C. In addition, the OFETs based on **P-BNBP-2CNTVT** show a lower threshold voltage (V_T) of about 25 V (V_T ~50 V for **P-BNBP-TVT**[13]) and leakage current (I_g) (Figure S7). All the above observations verified that cyano-functionalization could effectively down-shift the LUMO/HOMO energy levels. However, the causations for moderate electron mobility probably are attributed to the steric repulsion with neighboring BNBP units after the attachments of the cyano groups, which gives rise to distortion of the polymer backbone having been reported in the literatures.[16] In a word, we developed a new n-type semiconductor based on a BNBP unit using cyano-functionalization.

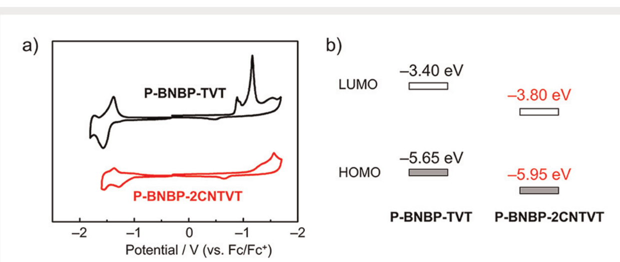

Figure 4 a) Cyclic voltammograms of **P-BNBP-TVT** and **P-BNBP-2CNTVT** in thin films (Fc/Fc$^+$ = ferrocene/ferrocenium); b) Schematic of their LUMO/HOMO energy level alignments.

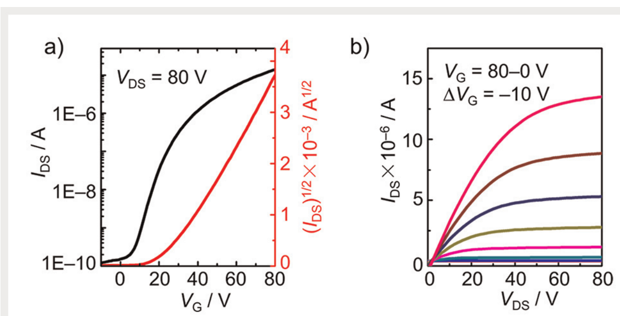

Figure 5 a) Transfer and b) output curves of the OFETs based on the **P-BNBP-2CNTVT** films annealed at 200 °C.

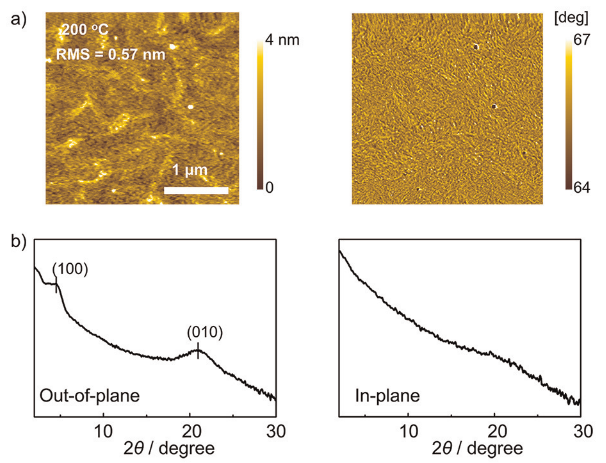

Figure 6 a) AFM high images and phase images for spin-coated **P-BNBP-2CNTVT** films annealed at 200 °C. b) GI-XRD patterns of the spin-coating films in the out-of-plane direction and the in-plane direction of **P-BNBP-2CNTVT** films.

Film Morphology and Microstructural Analysis. The film morphology of semiconductors plays a crucial role in OFETs' performance. We firstly performed atomic force microscopy (AFM) of **P-BNBP-2CNTVT** thin films to investigate the relationship between the film morphology and device performances. Figures 6a and S8 show the AFM height images and phase images of the **P-BNBP-2CNTVT** films after thermal annealing at different temperatures of 100, 200 and 300 °C. The **P-BNBP-2CNTVT** film annealed at 200 °C shows continuous and smooth film topography with the smallest root mean square surface roughness value of 0.57 nm, which indicates its enhanced film ordering, taking an account for the improved electron transport performance in the OFETs.[17]

We also utilized grazing incidence X-ray diffraction (GI-XRD) to clarify the polymer crystallinity and packing structure, which are closely associated with transport properties. The out-of-plane and in-plane XRDs of **P-BNBP-2CNTVT** films are displayed in Figures 6b and S9. The previous study reported that **P-BNBP-TVT** exhibits edge-on packing mode in thin films with a compact π–π stacking distance of 0.36 nm along the in-plane direction, which is beneficial to the interchain charge transport.[13] However, the **P-BNBP-2CNTVT** film gives a (100) diffraction peak at $2\theta = 4.5°$ and a (010) diffraction peak at $2\theta = 21.2°$ along the out-of-plane direction. Lamellar and π–π stacking distance based on the (100) and (010) diffraction peaks could be calculated to be 1.96 nm and 0.42 nm, respectively. And there are no obvious diffraction peaks in the in-plane direction. The large π–π stacking distance is not favorable for electron transport.[18] These results demonstrate that the introduction of cyano groups in polymer backbones causing steric hindrance has undesirable influences on the molecular packing, which gives the reason why **P-BNBP-2CNTVT** exhibits moderate electron mobilities.

Conclusions

In summary, we successfully synthesized a novel unipolar n-type transport polymer semiconductor based on a BNBP unit, **P-BNBP-2CNTVT**, where the cyano groups are decorated in the TVT moiety. In comparison to **P-BNBP-TVT** without cyano groups, the LUMO/HOMO energy levels of **P-BNBP-2CNTVT** dramatically down-shift by 0.4 eV and 0.3 eV, respectively, demonstrating the high electron affinity which are very desirable for electron injection. Thus, the OFETs based on **P-BNBP-2CNTVT** show unipolar n-type behavior with a moderate electron mobility of $0.026\ cm^2 \cdot V^{-1} \cdot s^{-1}$. Moreover, **P-BNBP-2CNTVT** manifests an unsatisfying π–π stacking distance up to 0.42 nm owing to the large steric hindrance after the incorporation of cyano groups, which gives an explanation for the moderate electron mobility. In a word, this study demonstrates that organoboron π-conjugated polymers could be regarded as a tool for constructing exclusive n-type semiconducting polymers used in OFETs. And we are convinced that the enhanced electron mobility of organoboron π-conjugated polymers could be realized through the optimizations of chemical structures and thin film morphology, and the further investigations are in progress in our lab.

Experimental Section

All reagents and solvents were purchased at reagent grade from commercial suppliers and were used without further purification unless otherwise noted. ^1H and ^{13}C NMR spectra were measured with a Bruker AV-400 (500 MHz for 1H and 126 MHz for ^{13}C) spectrometer in $CDCl_3$ and C_6D_6 at 25 °C or deuterated 1,1,2,2-tetrachloroethane ($C_2D_2Cl_4$) at 100 °C. Chemical shifts are reported in δ ppm using $CDCl_3$ (7.26 ppm), $C_2D_2Cl_4$ (5.98 ppm) and C_6D_6 (7.16 ppm) for ^1H NMR, as well as using $CDCl_3$ (77.16 ppm) for ^{13}C NMR as an internal standard. The molecular weights of the polymers were determined by gel permeation GPC on a PL-GPC 220-type at 150 °C. 1,2,4-Trichlorobenzene (TCB) was used as the eluent and monodisperse polystyrene was used as the standard. UV-vis absorption spectra were measured with a Shimadzu UV-3600 spectrometer. CV was performed on an CHI660a electrochemical workstation using Bu_4NClO_4 (0.1 M) in acetonitrile as the electrolyte solution and ferrocene as an internal reference at a scan rate of $50\ mV \cdot s^{-1}$. The CV cell consisted of a glassy carbon working electrode, a Pt wire counter electrode, and a standard calomel reference electrode. The polymer was casted on the working electrode for measurements. The redox potentials were calibrated with ferrocene as the standard. The HOMO and LUMO energy levels of the materials were estimated by the equations: $E_{HOMO}/E_{LUMO} = -(4.80 + E_{onset}^{ox}/E_{onset}^{red})$. Thermal analysis was performed on a Perkin-Elmer 7 instrument at a heating rate of 20 °C·min^{-1} under a nitrogen flow. AFM was performed with a SPA300HV (Seiko Instruments, Inc., Japan) in the tapping mode. GI-XRD data were obtained on a Bruker D8 Discover reflector (Cu Kα, λ = 1.54 056 Å) under 40 kV and 40 mA tube current. The scanning speed was 5 s per step with 0.05° step size (2*θ*). The measurement was obtained in a scanning interval of 2*θ* between 2° and 30°. The in-plane XRD profiles were obtained using a Rigaku SmartLab with an X-ray generation power of 40 kV tube voltage and 30 mA tube current. The diffraction was recorded in the 2*θ* – χ mode. The scanning speed was 5 s per step with 0.02° step size (2*θ*). The measurement was obtained in a scanning interval of 2*θ* between 2° and 30°.

Procedures

(*E*)-1,2-Bis(3-bromothiophen-2-yl)ethene

(*E*)-1,2-Bis(3-bromothiophen-2-yl)ethene was prepared using improved post-treatment methods with higher yield compared to references.[10] $TiCl_4$ (4.38 mL, 39.9 mmol) was added dropwise to a slurry of 3-bromothiophene-2-carbaldehyde **1** (5 g, 26.2 mmol) in THF (75 mL) with stirring at −18 °C. After stirring at this temperature for 30 min, Zn powders (5.2 g, 79.5 mmol) were divided into several equal parts and added in over a period of 30 min. The mixture was stirred at −18 °C for another 30 min, and then refluxed for 4 h. The reaction was quenched by adding ice-cold H_2O. The mixture was extracted with dichloromethane several times and dried over Na_2SO_4. The solvent was removed and purified by recrystallization from chloroform to give a pale brown solid. Yield: 57% (2.7 g). The ^{1}H NMR spectrum is consistent with the previous report.[10]

^{1}H NMR (500 MHz, $CDCl_3$, ppm): δ 7.20 (d, *J* = 5.4 Hz, 2 H), 7.12 (s, 2 H), 6.98 (d, *J* = 5.4 Hz, 2 H).

(*E*)-1,2-Bis(3-cyanothiophene-2-yl)ethene

A mixture of (*E*)-1,2-Bis(3-bromothiophen-2-yl)ethene (1.5 g, 4.28 mmol) and CuCN (1.92 g, 21.4 mmol) in anhydrous DMF (65 mL) was stirred for 24 h at 150 °C. Subsequently, it was allowed to cool to 70 °C. Then, $FeCl_3 \cdot 6H_2O$ (4.65 g, 17.14 mmol) in 2 M aqueous HCl (9 mL) was added and stirred at 70 °C for 1 h. Next the mixture was extracted with dichloromethane several times and dried over Na_2SO_4. The solvent was removed and purified by silica gel column chromatography using dichloromethane : petroleum (2 : 1 v/v) to obtain the desired compound as a yellow solid. Yield: 79% (0.82 g). The ^{1}H NMR spectrum is consistent with the previous report.[10]

^{1}H NMR (500 MHz, $CDCl_3$, ppm): δ 7.39 (s, 2 H), 7.35 (d, *J* = 5.1 Hz, 2 H), 7.22 (d, *J* = 5.1 Hz, 2 H).

(*E*)-1,2-Bis(5-(trimethylstannyl)-3-cyanothiophene-2-yl)ethene (2CNTVT)

2CNTVT was prepared according to references.[10] The fresh made LDA (1.0 M LDA, 2.42 mL, 2.42 mmol) was added dropwise at −78 °C to a solution of compound **3** (0.24 g, 1 mmol) in anhydrous THF (34 mL). After stirring for 1.5 h at −78 °C, trimethyltin chloride (0.6 g, 3 mmol) was added in one portion to the reaction mixture. Subsequently, the reaction flask was warmed to room temperature and stirred another 2 h. After the reaction finished, the mixture was quenched with distilled cold water and extracted with cold diethyl ether. The organic layer was dried over Na_2SO_4. After removing the solvents, the obtained residue was purified by recrystallization from ethanol to give a yellow product. Yield: 50% (0.28 g). The ^{1}H NMR spectrum is consistent with the previous report.[10]

^{1}H NMR (500 MHz, C_6D_6, ppm): δ 7.50 (s, 2 H), 6.72 (s, 2 H),0.11 (s, 18 H).

Polymer P-BNBP-2CNTVT

Starting materials of **BNBP** (100 mg, 0.075 mmol), **2CNTVT** (42.4 mg, 0.075 mmol), $Pd_2(dba)_3 \cdot CHCl_3$ (1.6 mg, 0.02 mmol) and P(*o*-Tolyl)$_3$ (3.6 mg, 0.16 mmol) were mixed under argon, and then dried toluene (7.5 mL) was added. The mixture was stirred at 120 °C for 24 h. After cooling, the solvent was dispersed in methanol and then the precipitate was collected. The obtained dark solid was purified by Soxhlet extraction using acetone, hexane and chloroform. The chloroform fraction was concentrated and poured into methanol, which were collected and dried in vacuum overnight. Yield: 100.0 mg (93%). GPC (TCB, polystyrene standard, 150 °C): M_n = 51 523, PDI = 1.91.

^{1}H NMR (400 MHz, $C_2D_2Cl_4$, 100 °C, ppm): δ 9.73 (s, 2 H), 9.05 (s, 2 H), 8.93 (s, 2 H), 8.89 (s, 2 H), 4.98 (s, 4 H), 3.25 (s, 2 H), 2.69–2.83 (m, 32 H), 2.60–2.64 (m, 80 H), 2.23(t, 12 H).

Device Fabrication and Characterization

TGBC OFETs were fabricated on silicon wafer covered with 300 nm SiO_2. The substrates were first cleaned with double-distilled water, acetone and isopropanol in an ultrasonic bath and then dried under a nitrogen flow. The substrates were heated to 120 °C for 1 hour and finally treated with a UV-ozone instrument for 15 min. First, Au source/drain electrodes (~25 nm) were deposited on cleaned bare Si/SiO_2 wafer with *W*/*L* = 70 (*W* = 5.6 mm, *L* = 80 µm). **P-BNBP-2CNTVT** was first dissolved in hot chloroform solutions (55 °C, 1 mg/mL) by stirring for 2 hours, and then aging for more than 8 hours. The polymer films were spin-coated on the substrates, followed by thermal annealing at 200 °C for 10 min. Then the solution of 80 mg/mL poly(methylmethacrylate) (PMMA) (product no. 182 230 from Aldrich, M_w = 120 kDa) in butyl acetate (~500 nm) as a dielectric was deposited by spin coating at 2000 rpm for 2 min and then annealed at 100 °C for 1 h. Finally, Al (~70 nm) was vacuum-deposited as a gate electrode. Field-effect mobility was extracted in the saturation regime by using the equation: $I_D^{sat} = (\mu C_i W/2L)(V_G - V_T)^2$, where I_D is the drain–source current, μ is the field-effect mobility, C_i is the capacitance per unit area of the gate dielectric layer (dielectric constant of PMMA, 500 nm, 5.5 nF/cm^2), and V_G and V_T are the gate voltage and threshold voltage, respectively.

Funding Information

This study was supported by the National Key Research and Development Program of China (2018YFE0 100 600) funded by MOST and Natural Science Foundation of China (No. 21 625 403, 21 875 244).

Supporting Information

Supporting Information for this article is available online at https://doi.org/10.1055/a-1639-2383.

Conflict of Interest

The authors declare no conflict of interest.

References

(1) Arias, A. C.; MacKenzie, J. D.; McCulloch, I.; Rivnay J.; Salleo, A. *Chem. Rev.* **2010**, *110*, 3.

(2) (a) Sirringhaus, H. *Adv. Mater.* **2014**, *26*, 1319; (b) Zhao, Y.; Guo, Y.; Liu, Y. *Adv. Mater.* **2013**, *25*, 5372; (c) Sun, H.; Liu, B.; Ma, Y.; Lee, J.-W.; Yang, J.; Wang, J.; Li, Y.; Li, B.; Feng, K.; Shi, Y.; Zhang, B.; Han, D.; Meng, H.; Niu, L.; Kim, B. J.; Zheng, Q.; Guo, X. *Adv. Mater.* **2021**. doi:10.1002/adma.202102635.

(3) (a) Kang, I.; Yun, H.-J.; Chung, D. S.; Kwon, S.-K.; Kim, Y.-H. *J. Am. Chem. Soc.* **2013**, *135*, 14896; (b) Back, J. Y.; Yu, H.; Song, I.; Kang, I.; Ahn, H.; Shin, T. J.; Kwon, S.-K.; Oh, J. H.; Kim, Y.-H. *Chem. Mater.* **2015**, *27*, 1732.

(4) Meijer, E. J.; de Leeuw, D. M.; Setayesh, S.; van Veenendaal, E.; Huisman, B. H.; Blom, P. W. M.; Hummelen, J. C.; Scherf, U.; Klapwijk, T. M. *Nat. Mater.* **2003**, *2*, 678.

(5) (a) Zhao, Z.; Yin, Z.; Chen, H.; Zheng, L.; Zhu, C.; Zhang, L.; Tan, S.; Wang, H.; Guo, Y.; Tang, Q.; Liu, Y. *Adv. Mater.* **2017**, *29*, 1602410; (b) Fei, Z.; Han, Y.; Martin, J.; Scholes, F. H.; Al-Hashimi, M.; Al-Qaradawi, S. Y.; Stingelin, N.; Anthopoulos, T. D.; Heeney, M. *Macromolecules* **2016**, *49*, 6384.

(6) (a) Gao, Y.; Zhang, X.; Tian, H.; Zhang, J.; Yan, D.; Geng, Y.; Wang, F. *Adv. Mater.* **2015**, *27*, 6753; (b) Gruber, M.; Jung, S.-H.; Schott, S.; Venkateshvaran, D.; Kronemeijer, A. J.; Andreasen, J. W.; McNeill, C. R.; Wong, W. W. H.; Shahid, M.; Heeney, M.; Lee, J.-K.; Sirringhaus, H. *Chem. Sci.* **2015**, *6*, 6949; (c) Yang, J.; Liu, Q.; Hu, M.; Ding, S.; Liu, J.; Wang, Y.; Liu, D.; Gao, H.; Hu, W.; Dong, H. *Sci. China Chem.* **2021**, *64*, 1410; (d) Liu, L.-N.; Li, Y.-P.; Khalil, M.; Xu, Z.-W.; Xie, G.; Zhang, X.; Li, J.; Li, W.-S. *Chin. J. Chem.* **2020**, *38*, 1663; (e) Yang, J.; Wang, H.; Chen, J.; Huang, J.; Jiang, Y.; Zhang, J.; Shi, L.; Sun, Y.; Wei, Z.; Yu, G.; Guo, Y.; Wang, S.; Liu, Y. *Adv. Mater.* **2017**, *29*, 1606162.

(7) (a) Gao, Y.; Deng, Y.; Tian, H.; Zhang, J.; Yan, D.; Geng, Y.; Wang, F. *Adv. Mater.* **2017**, *29*, 1606217; (b) Yang, J.; Zhao, Z.; Geng, H.; Cheng, C.; Chen, J.; Sun, Y.; Shi, L.; Yi, Y.; Shuai, Z.; Guo, Y.; Wang, S.; Liu, Y. *Adv. Mater.* **2017**, *29*, 1702115; (c) Kim, M.; Park, W.-T.; Park, S. A.; Park, C. W.; Ryu, S. U.; Lee, D. H.; Noh, Y.-Y.; Park, T. *Adv. Funct. Mater.* **2019**, *29*, 1805994; (d) Lei, T.; Cao, Y.; Fan, Y.; Liu, C.-J.; Yuan, S.-C.; Pei, J. *J. Am. Chem. Soc.* **2011**, *133*, 6099; (e) Xue, G.; Zhao, X.; Qu, G.; Xu, T.; Gumyusenge, A.; Zhang, Z.; Zhao, Y.; Diao, Y.; Li, H.; Mei, J. *ACS Appl. Mater. Interfaces* **2017**, *9*, 25426; (f) Lei, T.; Dou, J.-H.; Pei, J. *Adv. Mater.* **2012**, *24*, 6457.

(8) (a) Chen, Z.; Wei, X.; Huang, J.; Zhou, Y.; Zhang, W.; Pan, Y.; Yu, G. *ACS Appl. Mater. Interfaces* **2019**, *11*, 34171; (b) Chen, Z.; Zhang, W.; Huang, J.; Gao, D.; Wei, C.; Lin, Z.; Wang, L.; Yu, G. *Macromolecules* **2017**, *50*, 6098; (c) Sui, Y.; Shi, Y.; Deng, Y.; Li, R.; Bai, J.; Wang, Z.; Dang, Y.; Han, Y.; Kirby, N.; Ye, L.; Geng, Y. *Macromolecules* **2020**, *53*, 10147; (d) Wei, C.; Zhang, W.; Huang, J.; Li, H.; Zhou, Y.; Yu, G. *Macromolecules* **2019**, *52*, 2911; (e) Zheng, Y.-Q.; Lei, T.; Dou, J.-H.; Xia, X.; Wang, J.-Y.; Liu, C.-J.; Pei, J. *Adv. Mater.* **2016**, *28*, 7213.

(9) (a) Shi, S.; Wang, H.; Chen, P.; Uddin, M. A.; Wang, Y.; Tang, Y.; Guo, H.; Cheng, X.; Zhang, S.; Woo, H. Y.; Guo, X. *Polym. Chem.* **2018**, *9*, 3873; (b) Iguchi, K.; Mikie, T.; Saito, M.; Komeyama, K.; Seo, T.; Ie, Y.; Osaka, I. *Chem. Mater.* **2021**, *33*, 2218; (c) Wei, C.; Tang, Z.; Zhang, W.; Huang, J.; Zhou, Y.; Wang, L.; Yu, G. *Polym. Chem.* **2020**, *11*, 7340; (d) Yang, M.; Du, T.; Zhao, X.; Huang, X.; Pan, L.; Pang, S.; Tang, H.; Peng, Z.; Ye, L.; Deng, Y.; Sun, M.; Duan, C.; Huang, F.; Cao, Y. *Sci. China Chem.*, **2021**, *64*, 1219; (e) Han, W.; Wang, Z.; Hu, Y.; Yang, X.; Ge, C.; Gao, X. *Sci. China Chem.*, **2020**, *63*, 1182; (f) Casey, A.; Han, Y.; Fei, Z.; White, A. J. P.; Anthopoulos, T. D.; Heeney, M. *J. Mater. Chem. C* **2015**, *3*, 265; (g) Kim, H. G.; Kim, M.; Clement, J. A.; Lee, J.; Shin, J.; Hwang, H.; Sin, D. H.; Cho, K. *Chem. Mater.* **2015**, *27*, 6858.

(10) Kim, H. S.; Huseynova, G.; Noh, Y.-Y.; Hwang, D.-H. *Macromolecules* **2017**, *50*, 7550.

(11) (a) Yu, H.; Park, K. H.; Song, I.; Kim, M.-J.; Kim, Y.-H.; Oh, J. H. *J. Mater. Chem. C* **2015**, *3*, 11697; (b) Choi, H. H.; Baek, J. Y.; Song, E.; Kang, B.; Cho, K.; Kwon, S.-K.; Kim, Y.-H. *Adv. Mater.* **2015**, *27*, 3626; (c) Zhu, C.; Zhao, Z.; Chen, H.; Zheng, L.; Li, X.; Chen, J.; Sun, Y.; Liu, F.; Guo, Y.; Liu, Y. *J. Am. Chem. Soc.* **2017**, *139*, 17735.

(12) (a) Shin, J.; Um, H. A.; Lee, D. H.; Lee, T. W.; Cho, M. J.; Choi, D. H. *Polym. Chem.* **2013**, *4*, 5688; (b) Chen, H.; Guo, Y.; Yu, G.; Zhao, Y.; Zhang, J.; Gao, D.; Liu, H.; Liu, Y. *Adv. Mater.* **2012**, *24*, 4618.

(13) Long, X.; Gao, Y.; Tian, H.; Dou, C.; Yan, D.; Geng, Y.; Liu, J.; Wang, L. *Chem. Commun.* **2017**, *53*, 1649.

(14) (a) Sui, Y.; Deng, Y.; Han, Y.; Zhang, J.; Hu, W.; Geng, Y. *J. Mater. Chem. C* **2018**, *6*, 12896; (b) Lei, T.; Dou, J.-H.; Ma, Z.-J.; Yao, C.-H.; Liu, C.-J.; Wang, J.-Y.; Pei, J. *J. Am. Chem. Soc.* **2012**, *134*, 20025.

(15) (a) Newman, C. R.; Frisbie, C. D.; da Silva Filho, D. A.; Brédas, J.-L.; Ewbank, P. C.; Mann, K. R.; *Chem. Mater.* **2004**, *16*, 4436; (b) Nicolai, H. T.; Kuik, M.; Wetzelaer, G. A. H.; de Boer, B.; Campbell, C.; Risko, C.; Brédas, J. L.; Blom, P. W. M. *Nat. Mater.* **2012**, *11*, 882; (c) Chua, L.-L.; Zaumseil, J.; Chang, J.-F.; Ou, E. C. W.; Ho, P. K. H.; Sirringhaus, H.; Friend, R. H. *Nature* **2005**, *434*, 194. (d) Hauschild, M.; Borkowski, M.; Dral, P. O.; Marszalek, T.; Hampel, F.;

Xie, G.; Freudenberg, J.; Bunz, U. H. F.; Kivala, M. *Org. Mater.* **2020**, *02*, 204.

(16) (a) Lei, T.; Wang, J.-Y.; Pei, J. *Acc. Chem. Res.* **2014**, *47*, 1117; (b) Chochos, C. L.; Economopoulos, S. P.; Deimede, V.; Gregoriou, V. G.; Lloyd, M. T.; Malliaras, G. G.; Kallitsis, J. K. *J. Phys. Chem. C* **2007**, *111*, 10732; (c) Wang, H.; Huang, J.; Uddin, M. A.; Liu, B.; Chen, P.; Shi, S.; Tang, Y.; Xing, G.; Zhang, S.; Woo, H. Y.; Guo, H.; Guo, X. *ACS Appl. Mater. Interfaces* **2019**, *11*, 10089; (d) Yun, H.-J.; Kang, S.-J.; Xu, Y.; Kim, S. O.; Kim, Y.-H.; Noh, Y.-Y.; Kwon, S.-K. *Adv. Mater.* **2014**, *26*, 7300.

(17) (a) Wang, X.-Y.; Zhuang, F.-D.; Zhou, X.; Yang, D.-C.; Wang, J.-Y.; Pei, J. *J. Mater. Chem. C* **2014**, *2*, 8152; (b) Zhan, X.; Zhang, J.; Gong, Y.; Tang, S.; Tu, J.; Xie, Y.; Peng, Q.; Yu, G.; Li, Z. *Mater. Chem. Front.* **2017**, *1*, 2341.

(18) Zhao, R.; Min, Y.; Dou, C.; Lin, B.; Ma, W.; Liu, J.; Wang, L. *ACS Appl. Polym. Mater.* **2020**, *2*, 19.